JCTC Journal of Chemical Theory and Computation

pubs.acs.org/JCTC Article

Reduced Cost Computation and Exploitation of Accurate Radial Interaction Potentials for Barrier-Less Processes

Luigi Crisci, Bernardo Ballotta, Marco Mendolicchio, and Vincenzo Barone*

Cite This: https://doi.org/10.1021/acs.jctc.4c01076 Read Online

ACCESS | Metrics & More | Article Recommendations | Supporting Information

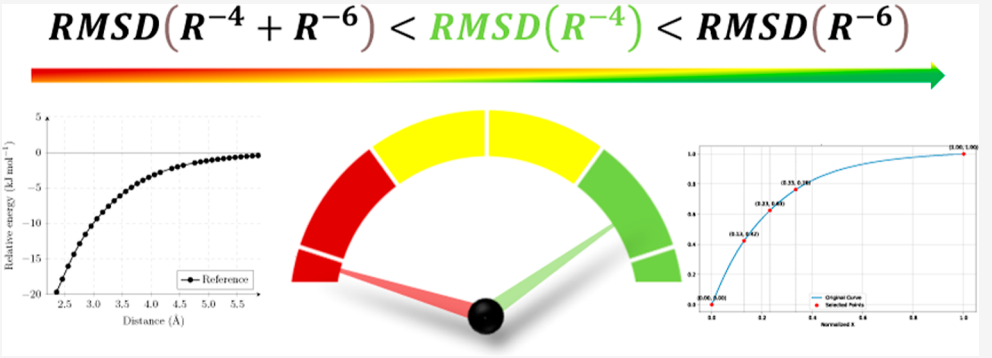

ABSTRACT: Barrier-less steps are typical of radical and ionic reactions in the gas-phase, which often take place in extreme environments such as the combustion reactors operating at very high temperatures or the interstellar medium, characterized by ultralow temperatures and pressures. The difficulty of experimental studies in conditions mimicking these environments suggests that computational approaches can provide a valuable support. In this connection, the most advanced treatments of these processes in the framework of transition state theory are able to deliver accurate kinetic parameters provided that the underlying potential energy surface is sufficiently accurate. Since this requires a balanced treatment of static and dynamic correlation (which play different roles in different regions), very sophisticated and expensive quantum chemical approaches are required. One effective solution of this problem is offered by the computation of accurate one-dimensional radial potentials, which are then used to correct the results of a Monte Carlo sampling performed by cheaper quantum chemical approaches. In this paper, we will show that, for a large panel of different barrier-less reaction steps, the radial potential is ruled by the R^{-4} term and that addition of a further R^{-6} contribution provides quantitative agreement with the reference points. The consequences of this outcome are not trivial, since the reference potential can be fitted by a very limited number of points possibly with a nonlinear spacing. In the case of reaction steps ruled by long-range transition states, generalized expressions are also given for computing reaction rates in the framework of the phase-space theory. All these improvements pave the way toward the computation of reaction rates for barrier-less reactions involving large molecules.

1. INTRODUCTION

Barrier-less reaction steps play a pivotal role in a variety of chemical environments including the interstellar medium (ISM),[1−4] planet atmospheres,[5−8] and combustion reactors.[9−11] In such cases, the transition state (TS) does not correspond to a potential energy barrier, but is related to a minimum in the number of available ro-vibrational states for motions perpendicular to a suitable reaction coordinate.[12,13] Generally, there are two reasonably distinct TS regions,[14−18] which are ruled by different kinds of interactions.[13] The "outer" TS lies in the region of the centrifugal barriers on the long-range tail of the potential energy surface (PES).[19,20] On the other hand, an "inner" TS generally arises in the region where covalent bonding and steric repulsions are comparable to or, even larger than, multipolar, dispersion, and/or van der Waals interactions.[21,22] In the ISM, the "outer" region usually plays a dominant role, whereas at the high temperatures characterizing combustion reactors the "inner" region is more important. The transition between those two regimes occurs at temperatures around 100 K,[21] so that both TSs play a significant role in reactions occurring in the Earth atmosphere.

One of the most successful approaches for obtaining reliable reaction rates for all these kinds of processes is the variable reaction coordinate (VRC)[22−24] extension of the TS theory (TST),[25] which is based on an extensive Monte Carlo (MC)[26]

Received: August 17, 2024
Revised: October 16, 2024
Accepted: October 17, 2024

sampling of the transitional (interfragment)[27−29] degrees of freedom to determine dividing surfaces on the PES (in terms of the values and forms of suitable reaction coordinates), i.e., hypersurfaces that minimize the reactive fluxes. The huge number of energy evaluations required by this approach forces the use of relatively cheap quantum chemical methods [hereafter broadly referred to as low-level (LL) methods],[30] whose accuracy is, however, generally not sufficient for obtaining quantitative results, especially when multireference descriptions are needed (a typical situation for homolytic bond breaking processes). Under such circumstances, a radial reference potential obtained by a high-level (HL) method can be profitably employed to correct the LL results.[30−34] Furthermore, an isotropic radial potential is employed in the capture theories, which are still widely employed to describe barrier-less steps in astrochemical reactions.[3,4]

The computation and analytical representation of such reference potentials is the main topic of the present paper. As already mentioned, huge computational efforts are needed to obtain accurate energies for a large number of points involving significant nondynamical correlation and, above all, the prohibitive scaling of state-of-the-art methods with the dimensions of the investigated systems precludes their brute-force use for medium- to large-sized molecules. Therefore, we have developed reduced-cost composite schemes,[35,36] which increase the size of systems amenable to accurate investigations, and, more recently,[33] we have introduced the combined use of these methods for the computation of the high-spin state of a multiplet with the difference dedicated configuration interaction (DDCI) approach[37−41] for computing the spin splitting between this state and its low-spin (LS) counterparts. These methods have been used in the present paper to compute radial reference potentials for 20 representative reactions, which were then fitted by polynomials of the inverse distance (R) between the closest atoms belonging to different fragments. The general trends shown by these prototypical systems could hopefully allow the definition of a general and robust unsupervised protocol for the study of reactive systems of large dimensions.

The paper is organized as follows. After a summary of the main aspects of the theoretical background, the role of radial potentials in computational kinetics is discussed, and some generalizations of the current approaches are given. Then, after providing the essential details of the composite methods employed in the reference quantum chemical computations, the results obtained for prototypical reactions are analyzed, and different fittings and selections of sampling points are compared, leading to a general effective recipe. Finally, conclusions and perspectives are given in the last section.

2. THEORETICAL BACKGROUND

As is well-known, the long-range interaction between an ion and a neutral molecule is ruled by a R^{-4} interaction, whereas the interaction between a polar molecule and a neutral one is led by a R^{-6} dependence, and the interaction between the quadrupole moment of one molecule and the induced dipole of another one is characterized by a R^{-8} leading term.[42] Therefore, when strong electrostatic interactions are not present, the long-range radial potential governing these processes should be well described by a polynomial of the inverse distance containing only even powers

$$V(R) = -\frac{C_2}{R^2} - \frac{C_4}{R^4} - \frac{C_6}{R^6} - \frac{C_8}{R^8} \tag{1}$$

with reference to the energy of the dissociated fragments. While the physical interpretation of the different terms becomes questionable for medium-range distances, we will show that eq 1 effectively captures the most significant contributions necessary for an accurate fit of the radial potentials ruling all the barrier-less reaction steps examined in the present study.

When a single term (with power n) dominates eq 1, the reactive event is effectively reduced to an atom−atom collision, and the following explicit expression of the canonical rate constant is obtained[21,43]

$$k(T) = (8\pi)^{1/2}\left(\frac{n-2}{2}\right)^{2/n}\Gamma(1-2/n)\mu^{-1/2}C_n T^{1/2-2/n} \tag{2}$$

where Γ is the Euler's gamma function, μ the reduced mass and T the absolute temperature. The well-known Langevin[44] and Gorin[45−47] expressions can be recovered setting $n = 4$ or $n = 6$ in eq 2. Actually, when the leading interactions corresponds to a single multipolar or dispersion (R^{-6}) interaction, a generalized equation can be derived in the framework of the so-called long-range TST, which includes also the relative orientations of the reacting moieties.[21] Here, we will not follow this route since the radial potential obtained by explicit quantum chemical computations will be used for both "outer" and "inner" TSs, with the latter one being poorly described by any one-center multipolar approximation. On the other hand, the microcanonical rate constant for the general case of eq 1 can be obtained taking into account that the "outer" TS is determined by the presence of a centrifugal term, which accounts for the relative orbital motion of the two fragments. This leads to the following effective interaction potential

$$V_{\text{eff}}(R) = \frac{L^2}{2\mu R^2} - \sum_n \frac{C_n}{R^n} \tag{3}$$

The angular momentum L can be written as

$$L = \mu v_r b \tag{4}$$

where v_r the relative velocity of the colliding species, and b the impact parameter.[48]

Then the relative translational energy E_{rel}, can be expressed in terms of μ and v_r

$$E_{\text{rel}} = \frac{\mu v_r^2}{2} \tag{5}$$

It is possible to rewrite the effective interaction potential as a function of the impact parameter b, i.e., the distance of closest approach between the two molecules in the absence of short-range interparticle forces

$$V_{\text{eff}}(R) = E_{\text{rel}}\left(\frac{b}{R}\right)^2 - \sum_n \frac{C_n}{R^n} \tag{6}$$

When the mean free path of the colliding particles is much larger than their sizes (i.e., in the free molecular regime) the state-selected rate constant k_{ij} and the reaction cross section σ_{ij} are related by the following expression[49]

$$k_{ij}(v_r) = \sigma_{ij} v_r \tag{7}$$

https://doi.org/10.1021/acs.jctc.4c01076
J. Chem. Theory Comput. XXXX, XXX, XXX−XXX

Then, for the thermodynamic regimes in which eq 7 is applicable, the average reaction cross section σ_r is obtained by averaging over all the internal states of the reactants

$$\sigma_r = \sum_{i,j} w_i^A w_j^B \sigma_{ij}(v_r) \tag{8}$$

where w_i^A and w_j^B are the Boltzmann weighting factors of the ith and jth reactant's internal states, respectively. The thermal rate constant $[k(T)]$ of processes governed by equilibrium Maxwell−Boltzmann distributions for the relative velocity of the fragments (v_r) is obtained by averaging $v_r\sigma_r$

$$k(T) = \left(\frac{8\beta^3}{\pi\mu}\right)^{1/2} \int_0^\infty dE_{rel} E_{rel} \sigma_r(E_{rel})\, e^{-\beta E_{rel}} \tag{9}$$

where β is $1/k_B T$ and k_B is Boltzmann's constant.

The reaction probability P_R can be expressed as a function of the impact parameter b. Since P_R decreases to zero for large b, we can introduce a value of $b = b_{max}$ after which the reaction probability is negligible. Then, the reaction cross-section is given by

$$\sigma_r = 2\pi \int_0^{b_{max}} P_R(b) b\, db \tag{10}$$

The simplest model assumes that the reactants do not interact with each other if the intermolecular distance is larger than a critical radius R^* [i.e., $P_R(b > R^*) = 0$], whereas they react at all shorter distances [i.e., $P_R(b \le R^*) = 1$].[12] In this case the reaction cross section can be rewritten as a function of the critical impact parameter $b_* = R^*$

$$\sigma_r = \pi b_*^2 \tag{11}$$

where b_* can be derived from the condition $dV_{eff}(R)/dR = 0$. Furthermore, eq 9 can be written in terms of the thermally averaged value of the relative velocity

$$v_r = \left(\frac{8}{\pi\mu\beta}\right)^{1/2} \tag{12}$$

Under these assumptions, eq 2 is obtained for the canonical rate constant of a reaction governed by a single-term radial potential. On the other hand, the gradient of the more general eq 1 vanishes when

$$2C_2R^6 + 3C_4R^4 + 6C_6R^2 + 8C_8 = 0 \tag{13}$$

Introducing the following change of variables

$$R^2 = y - \frac{2C_4}{3C_2} \tag{14}$$

Equation 13 can be rewritten in the well-known depressed form

$$y^3 + Py + Q = 0 \tag{15}$$

with

$$P = \frac{3C_6}{C_2} - \frac{4C_4^2}{3C_2^2} \qquad Q = \frac{4C_8}{C_2} - \frac{2C_4C_6}{C_2^2} + \frac{16C_4^3}{27C_2^3} \tag{16}$$

Solution of eq 15 may lead to one or three different real roots, depending on the value of the discriminant $\Delta = -4P^3 - 27Q^2$. When $\Delta > 0$, the cubic equation yields three distinct roots given by the following expression

$$y_n = 2\sqrt{-\frac{P}{3}}\cos\left[\frac{1}{3}\arccos\left(\frac{3Q}{2P}\sqrt{-\frac{3}{P}}\right) - \frac{2\pi n}{3}\right] \quad \text{with} \quad n = 0, 1, 2 \tag{17}$$

Conversely, when $\Delta < 0$ only one real solution is obtained, whose value depends on the sign of P

$$y_1 = \begin{cases} -2\dfrac{|Q|}{Q}\sqrt{-\dfrac{P}{3}}\cosh\left[\dfrac{1}{3}\operatorname{arccosh}\left(-\dfrac{3|Q|}{2P}\sqrt{-\dfrac{3}{P}}\right)\right] & \text{if } P < 0 \\ -2\sqrt{\dfrac{P}{3}}\sinh\left[\dfrac{1}{3}\operatorname{arcsinh}\left(\dfrac{3Q}{2P}\sqrt{\dfrac{3}{P}}\right)\right] & \text{if } P > 0 \end{cases} \tag{18}$$

Finally, when $\Delta = 0$, the equation has the following solutions

$$y_1 = \frac{3Q}{P} \qquad y_2 = y_3 = -\frac{3Q}{2P} \tag{19}$$

Let us recall that due to eq 14, $y_k - 2C_4/3C_2$ must be greater than or equal to zero, so that the kth value of R, from now on referred to as R_k, can be retrieved

$$R_k = \sqrt{y_k - \frac{2C_4}{3C_2}} \tag{20}$$

In principle, the impact parameter b_* can be associated with any possible stationary point of the potential $V_{eff}(R)$, i.e. with any value of R_k. However, it is worth mentioning that due to the relative order of magnitude of the C_n coefficients, solution of eq 15 leads in general to a single real and acceptable value of R_k, which will be referred to simply as b_* in the following. Of course, analytical equations can be straightforwardly derived also for radial potentials containing only two (e.g., C_4 and C_6) contributions, whereas eq 2 gives the thermal rate constant for the well-known one-term expansions of the radial potential.[21,44,45] In any case, once the radius R_k is known, it is possible to derive analytical expressions for the cross section σ_r and the microcanonical rate constant $k(E)$

$$\sigma_r = \pi\frac{b_*^2}{E_{rel}}\left(E + \frac{C_4}{b_*^4} + \frac{C_6}{b_*^6} + \frac{C_8}{b_*^8}\right) \tag{21}$$

$$k(E) = \pi\sqrt{\frac{2}{\mu E}}\left(Eb_*^2 + \frac{C_4}{b_*^2} + \frac{C_6}{b_*^4} + \frac{C_8}{b_*^6}\right) \tag{22}$$

In summary, for reactions governed by long-range TSs (e.g., at the very low-temperatures characterizing the ISM) rate constants can be derived from the capture theory by means of radial potentials obtained employing quantum chemical computations and fitted to polynomials of the squared inverse-distance between the closest atoms belonging to different fragments. More generally, the computed radial potentials can be employed to correct the results of cheaper quantum chemical methods for the MC sampling required by the VRC-TST model. Based on these premises, in the following sections we will analyze the radial potentials for a large panel of prototypical barrier-less reaction steps.

https://doi.org/10.1021/acs.jctc.4c01076
J. Chem. Theory Comput. XXXX, XXX, XXX−XXX

2.1. Quantum Chemical Radial Potentials. The behavior of different reaction channels can be classified qualitatively in terms of the number of electrons occupying the frontier orbitals of the interacting fragments. The situations with one or three electrons (radical−ion or radical−molecule) are usually dominated by a well-defined Slater determinant (i.e., occupation scheme), and this is also the case for four electrons, albeit in this situation, dispersion interactions play a dominant role. The case of two electrons leading to homolytic bond dissociation is more involved since, at intermediate distances, even a qualitative modeling requires a two-determinant description.

Single-reference approaches provide an accurate description of all the spin-paired singlet and the triplet (high-spin, HS) states. Therefore, their energies are computed by the jun-ChS-F12[35] or CPCS3[36,50] composite schemes, which include the following contributions

$$E = E_{V2} + \Delta E_V + \Delta E_{CV2} \tag{23}$$

where

$$E_{V2} = \frac{4^3 E(\text{fc-MP2/4Z}) - 3^3 E(\text{fc-MP2/3Z})}{4^3 - 3^3} \tag{24}$$

$$\Delta E_V = \frac{3^3 \Delta E(3Z) - 2^3 \Delta E(2Z)}{3^3 - 2^3} \tag{25}$$

with

$$\Delta E(\text{nZ}) = E(\text{fc-CCSD(T)/nZ}) - E(\text{fc-MP2/nZ}) \tag{26}$$

and

$$\Delta E_{CV2} = E(\text{ae-MP2/wC3}) - E(\text{fc-MP2/wC3}) \tag{27}$$

In this context, ae and fc refer to all-electron and frozen core, respectively, while wC3 and nZ denote cc-pwCVTZ[51] and jun-cc-pVTZ[52] (jun-ChS-F12) or cc-pVNZ-F12[53] (CPCS3) basis sets. Furthermore, either conventional (CPCS3) or explicitly correlated (jun-ChS-F12) post-Hartree−Fock approaches can be employed. Finally, post-MP2 CBS extrapolation is neglected in the jun-ChS-F12 model, so that eq 25 reduces to $\Delta E_V = \Delta E(3Z)$. Several works have shown that both composite schemes provide very accurate results for systems not involving strong nondynamical correlation,[35,54] and the choice of the specific method has been performed to permit a direct comparison with previous works providing all the details of the studied reactions.

When strong nondynamical correlation comes into play, instead of computing directly the energy of the LS electronic state, it is much more convenient to compute the energy difference (spin splitting) between different components of the spin multiplet (in the present case singlet and triplet).[55] In fact, the different components have very similar dynamic correlation, which is well approximated by the single-reference value for the triplet state. Then, static correlation and residual dynamic correlation can be computed accurately by dedicated difference approaches, which employ a reduced number of excitation classes.[33,39,56,57] In the present context, the MOLPRO[58] software is used to perform the DDCI computations, by combining the MRCI and MATROP modules and employing the cc-pVTZ-F12 basis set. The initial guess for the iterative version of DDCI employed here is obtained from a state-averaged CAS-SCF computation, which includes only the orbitals defining the spin multiplet (two in the present case) in a minimal active space. At the end of each cycle, the singlet−triplet energy gap is evaluated and compared to the previous one. If the difference is larger than the predefined threshold (1 kJ/mol), a state-averaged density matrix is generated and diagonalized. The number of active orbitals is then increased by one, and the procedure is repeated using as initial guess the state-averaged density matrix built from the natural orbitals of the previous iteration.

This iterative/black-box method yields the difference between HS and LS states, and the final energy is given by

$$E_{LS} = E_{HS}^{SR} - \Delta E_{HS-LS}^{DDCI} \tag{28}$$

where E_{HS}^{SR} is obtained by a generic single-reference method (CPCS3 in the present context).

Based on previous experience,[59−62] the geometries employed for single-point energy evaluations by HL methods (jun-ChS-F12, CPCS3, or DDCI) have been obtained by the double hybrid rev-DSD-PBEP86 hybrid functional[63] in conjunction with the jun-cc-pVTZ basis set[52] employing the Gaussian suite of programs.[64]

3. RESULTS AND DISCUSSION

The following 20 barrier-less elementary reaction steps have been selected in order to cover ion−molecule, radical−molecule, and radical−radical prototypical cases.

$$CH_3COOH + [NH_2]^+ \rightarrow [CH_3COHO\cdots NH_2]^+ \tag{R1}$$

$$[NH_2OH_2]^+ + HCONH_2 \rightarrow [NH_2OH - H\cdots OCHNH_2]^+ \tag{R2}$$

$$C_2H_4 \rightarrow C_2H_3 + H \tag{R3}$$

$$CH_4 \rightarrow CH_3 + H \tag{R4}$$

$$H_2S + Cl \rightarrow HSH\cdots Cl \tag{R5}$$

$$H_2S + OH \rightarrow HSH\cdots OH \tag{R6}$$

$$CH_2CHOH(\text{anti}) + OH \rightarrow CH_2CHO - H(\text{anti})\cdots O - H \tag{R7}$$

$$CH_2CHOH(\text{anti}) + OH \rightarrow H_2C{=}CHOH(\text{anti})\cdots O - H \tag{R8}$$

$$CH_2CHOH(\text{anti}) + OH \rightarrow CH_2CHH - O(\text{anti})\cdots H - O \tag{R9}$$

$$CH_2CHOH(\text{syn}) + OH \rightarrow H_2C{=}CHOH\cdots H - O \tag{R10}$$

$$CH_2CHOH(\text{syn}) + OH \rightarrow H_2C{=}CHOH(\text{syn})\cdots O - H \tag{R11}$$

$$CH_2CHOH(\text{syn}) + OH \rightarrow H_2C{=}CHOH(\text{syn})\cdots H - O \tag{R12}$$

$$(\text{E-})CH_3CHCHOH + OH \rightarrow (\text{E-})CH_3CHCHO - H\cdots O - H \tag{R13}$$

https://doi.org/10.1021/acs.jctc.4c01076
J. Chem. Theory Comput. XXXX, XXX, XXX−XXX

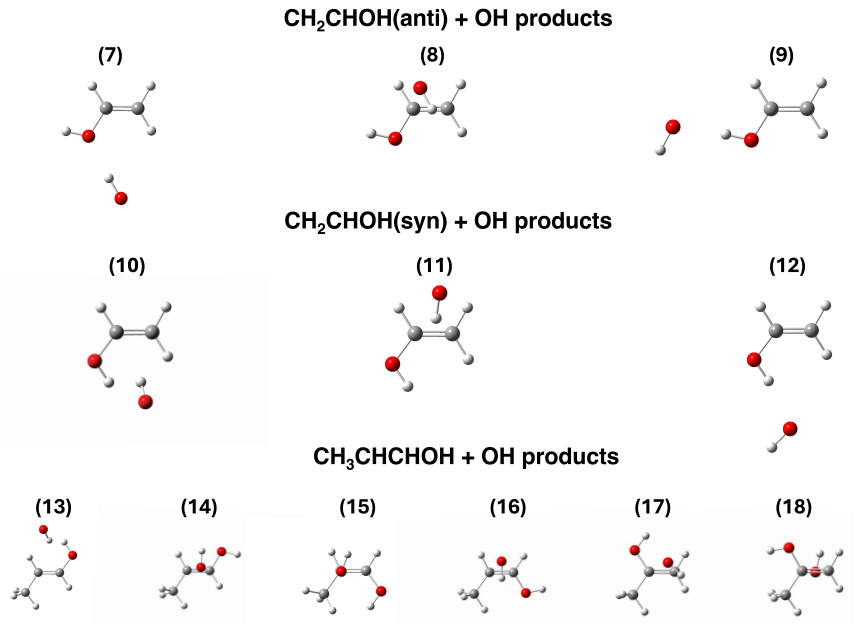

Figure 1. Ball-and-stick representations of the products for a subset of reactions, with the corresponding reaction index displayed above each structure.

Table 1. Root Mean Square Deviations (RMSD) Obtained by Different Fittings of the Quantum Chemical Radial Potentials for the 20 Prototypical Barrier-Less Reaction Steps Analyzed in the Present Work

Reaction	RMSD (kJ/mol)				
	R^{-6}	$R^{-6} + R^{-8}$	$R^{-4} + R^{-6} + R^{-8}$	R^{-4}	$R^{-4} + R^{-6}$
$CH_3COOH + [NH_2]^+ \rightarrow [CH_3COHO\cdots NH_2]^+$ reac. 1	0.00275	0.00275	0.00107	0.00107	0.00107
$[NH_2OH_2]^+ + HCONH_2 \rightarrow [NH_2OH-H\cdots OCHNH_2]^+$ reac. 2	0.01128	0.01128	0.00702	0.00702	0.00702
$C_2H_4 \rightarrow C_2H_3 + H$ reac. 3	0.00410	0.00410	0.00209	0.00248	0.00209
$CH_4 \rightarrow CH_3 + H$ reac. 4	0.00418	0.00418	0.00239	0.00292	0.00239
$H_2S + Cl \rightarrow HSH\cdots Cl$ reac. 5	0.00007	0.00006	0.00006	0.00034	0.00007
$H_2S + OH \rightarrow HSH\cdots OH$ reac. 6	0.00016	0.00016	0.00004	0.00015	0.00004
$CH_2CHOH(anti) + OH \rightarrow CH_2CHO-H(anti)\cdots O-H$ reac. 7	0.00174	0.00174	0.00101	0.00101	0.00101
$CH_2CHOH(anti) + OH \rightarrow H_2C{=}CHOH(anti)\cdots O-H$ reac. 8	0.00065	0.00065	0.00025	0.00025	0.00025
$CH_2CHOH(anti) + OH \rightarrow CH_2CHH-O(anti)\cdots H-O$ reac. 9	0.00145	0.00145	0.00083	0.00083	0.00083
$CH_2CHOH(syn) + OH \rightarrow H_2C{=}CHOH\cdots H-O$ reac. 10	0.00088	0.00088	0.00032	0.00032	0.00032
$CH_2CHOH(syn) + OH \rightarrow H_2C{=}CHOH(syn)\cdots O-H$ reac. 11	0.00048	0.00048	0.00021	0.00021	0.00021
$CH_2CHOH(syn) + OH \rightarrow H_2C{=}CHOH(syn)\cdots H-O$ reac. 12	0.00081	0.00081	0.00033	0.00033	0.00033
$(E\text{-})CH_3CHCHOH + OH \rightarrow (E\text{-})CH_3CHCHO-H\cdots O-H$ reac. 13	0.00124	0.00124	0.00059	0.00059	0.00059
$(Z\text{-})CH_3CHCHOH + OH \rightarrow (Z\text{-})CH_3CHCHO-H\cdots O-H$ reac. 14	0.00101	0.00101	0.00036	0.00036	0.00036
$(E)\text{-}CH_3CHCHOH + OH \rightarrow (E)\text{-}CH_3HC{=}CHOH\cdots O-H$ reac. 15	0.00089	0.00089	0.00032	0.00032	0.00032
$(Z)\text{-}CH_3CHCHOH + OH \rightarrow (Z)\text{-}CH_3HC{=}CHOH\cdots O-H$ reac. 16	0.00098	0.00098	0.00039	0.00039	0.00039
$CH_3OHCCH_2 + OH \rightarrow CH_3OHC{=}CH_2\cdots O-H$ reac. 17	0.00152	0.00152	0.00071	0.00071	0.00071
$CH_3OHCCH_2 + OH \rightarrow CH_3OHC{=}CH_2\cdots O-H$ reac. 18	0.00110	0.00110	0.00044	0.00044	0.00044
$HOHCCH_2(syn) + CN \rightarrow HOHC-CH_2(syn)\cdots CN$ reac. 19	0.00012	0.00011	0.00011	0.00090	0.00012
$HOHCCH_2(anti) + CN \rightarrow HOHCCH_2(anti)\cdots CN$ reac. 20	0.00014	0.00014	0.00010	0.00045	0.00010

$$(Z\text{-})CH_3CHCHOH + OH \rightarrow (Z\text{-})CH_3CHCHO - H\cdots O - H \quad \text{(R14)}$$

$$(E)\text{-}CH_3CHCHOH + OH \rightarrow (E)\text{-}CH_3HC{=}CHOH\cdots O - H \quad \text{(R15)}$$

$$(Z)\text{-}CH_3CHCHOH + OH \rightarrow (Z)\text{-}CH_3HC{=}CHOH\cdots O - H \quad \text{(R16)}$$

$$CH_3OHCCH_2 + OH \rightarrow CH_3OHC{=}CH_2\cdots O - H \quad \text{(R17)}$$

$$CH_3OHCCH_2 + OH \rightarrow CH_3OHC{=}CH_2\cdots O - H \quad \text{(R18)}$$

$$HOHCCH_2(syn) + CN \rightarrow HOHC - CH_2(syn)\cdots CN \quad \text{(R19)}$$

$$HOHCCH_2(anti) + CN \rightarrow HOHCCH_2(anti)\cdots CN \quad \text{(R20)}$$

https://doi.org/10.1021/acs.jctc.4c01076
J. Chem. Theory Comput. XXXX, XXX, XXX−XXX

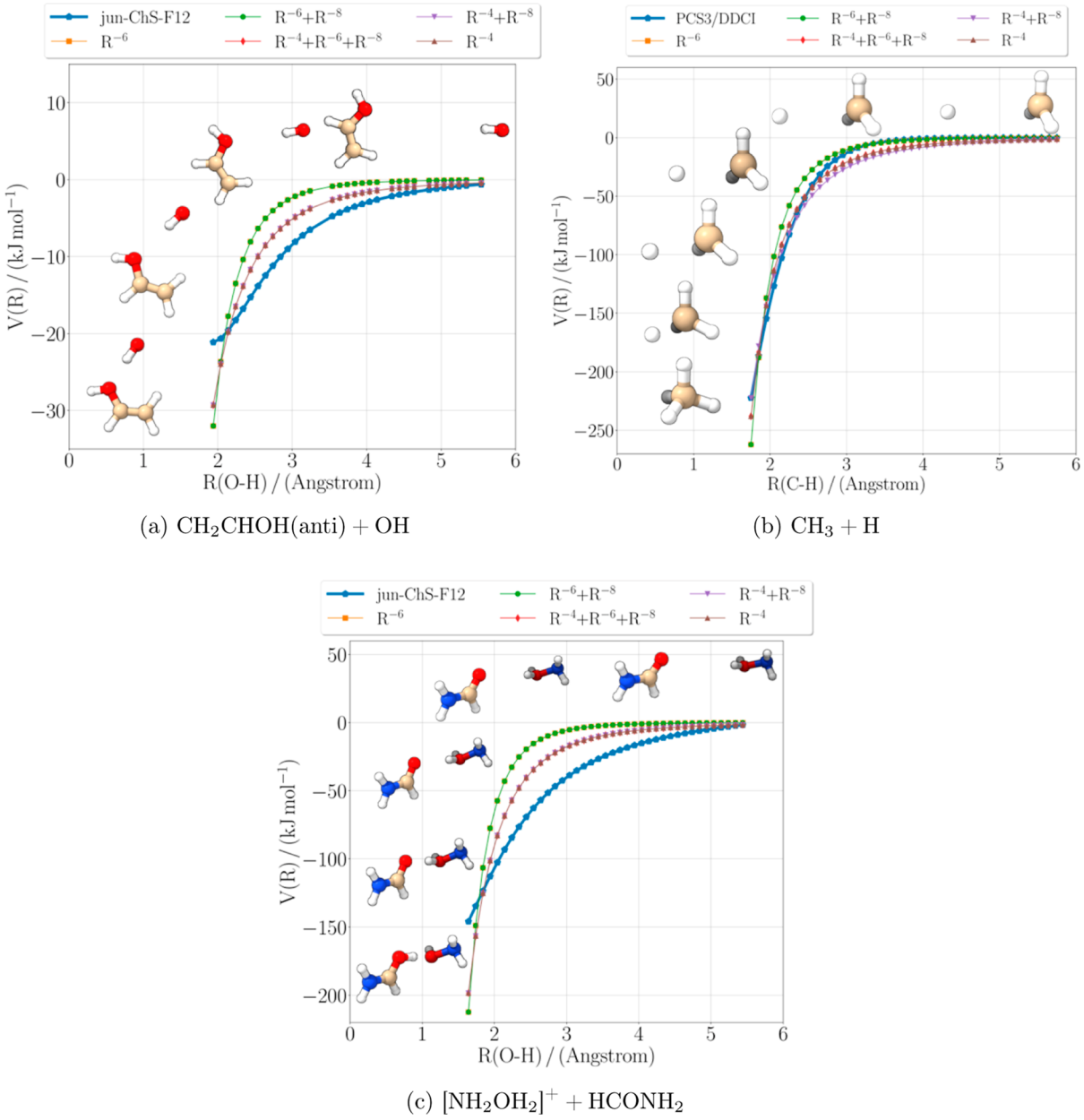

Figure 2. Relative fragment orientations and binding energies in kJ/mol as a function of the distance in Å between the closest atoms belonging to different fragments for reac. 7 (a), reac. 4 (b), and reac. 2 (c). The fittings with different polynomials of the squared inverse distance are also shown. See main text for further details.

Ball-and-stick representations of the products are shown in Figure 1 for possibly ambiguous situations.

For each reaction, starting from the equilibrium distance, a relaxed scan is performed in which all the geometrical parameters are optimized at the revDSD-PBEPB86/jun-cc-pVTZ level for fixed values of the distance between the closest atoms belonging to different fragments. An average of 40 points is employed for each reaction with a step-size of 0.1 Å.

Since most of those reactions have been analyzed in previous works,[65−73] a detailed discussion of their characteristic features will not be repeated here. We only point out that, for purposes of homogeneity, all the reactions have been now treated at the jun-ChS-F12 level, except the dissociation of CH_4 and C_2H_4, whose multireference character has required CPCS3/DDCI computations. Detailed results are given in the Supporting Information, whereas Table 1 collects the error statistics for different fittings of the quantum chemical potentials and Figure 2 sketches the trends of different interpolations for three prototypical cases, namely, a radical−molecule (reac. 7), a ion−molecule (reac. 2) and a radical−radical (reac. 4) reaction. Note that some curves are superimposed in Figure 2 since some initial choices of the radial expansions produced one or more vanishing coefficients in the least-squares fitting (see Supporting Information for details).

Those results have led to the choices summarized in Table 2. It is quite apparent that in most case a single-term expansion is sufficient to obtain accurate results, with the R^{-4} contribution always producing a good fit. As a matter of fact, two term (R^{-4} and R^{-6}) expansions produce marginally better results only in three cases (H_2S + OH and the multireference dissociations of CH_4 and C_2H_4), and three-term expansions are never required. It can be concluded that, for simple reactions, a careful choice

https://doi.org/10.1021/acs.jctc.4c01076
J. Chem. Theory Comput. XXXX, XXX, XXX−XXX

Table 2. Summary of the Most Accurate Functional Forms for the 20 Reactions Analyzed in the Present Work

reaction	most accurate fit	coefficient values
	Ion Molecule	
$CH_3COOH + [NH_2]^+ \rightarrow [CH_3COHO\cdots NH_2]^+$ reac. 1	R^{-4}	0.537322 (Å^4·(kJ/mol))
$[NH_2OH_2]^+ + HCONH_2 \rightarrow [NH_2OH{-}H\cdots OCHNH_2]^+$ reac. 2	R^{-4}	0.546689 (Å^4·(kJ/mol))
	Radical−Radical	
$C_2H_4 \rightarrow C_2H_3 + H$ reac. 3	$R^{-4} + R^{-6}$	0.701797 (Å^4·(kJ/mol)) + 1.066564 (Å^6·(kJ/mol))
$CH_4 \rightarrow CH_3 + H$ reac. 4	$R^{-4} + R^{-6}$	0.538338 (Å^4·(kJ/mol)) + 0.956110 (Å^6·(kJ/mol))
	Radical Molecule	
$H_2S + Cl \rightarrow HSH\cdots Cl$ reac. 5	R^{-4}	0.521679 (Å^4·(kJ/mol))
$H_2S + OH \rightarrow HSH\cdots OH$ reac. 6	$R^{-4} + R^{-6}$	0.463450 (Å^4·(kJ/mol)) + 8.484035 (Å^6·(kJ/mol))
$CH_2CHOH(anti) + OH \rightarrow CH_2CHO{-}H(anti)\cdots O{-}H$ reac. 7	R^{-6}	0.647928 Å^6·(kJ/mol)
$CH_2CHOH(anti) + OH \rightarrow H_2C{=}CHOH(anti)\cdots O{-}H$ reac. 8	R^{-6}	2.492211 Å^6·(kJ/mol)
$CH_2CHOH(anti) + OH \rightarrow CH_2CHH{-}O(anti)\cdots H{-}O$ reac. 9	R^{-6}	0.610354 Å^6·(kJ/mol)
$CH_2CHOH(syn) + OH \rightarrow H_2C{=}CHOH\cdots H{-}O$ reac. 10	R^{-4}	0.682832 (Å^4·(kJ/mol))
$CH_2CHOH(syn) + OH \rightarrow H_2C{=}CHOH(syn)\cdots O{-}H$ reac. 11	R^{-4}	0.343464 (Å^4·(kJ/mol))
$CH_2CHOH(syn) + OH \rightarrow H_2C{=}CHOH(syn)\cdots H{-}O$ reac. 12	R^{-4}	1.492152 (Å^4·(kJ/mol))
$(E\text{-})CH_3CHCHOH + OH \rightarrow (E\text{-})CH_3CHCHO{-}H\cdots O{-}H$ reac. 13	R^{-4}	0.679844 (Å^4·(kJ/mol))
$(Z\text{-})CH_3CHCHOH + OH \rightarrow (Z\text{-})CH_3CHCHO{-}H\cdots O{-}H$ reac. 14	R^{-4}	0.329527 (Å^4·(kJ/mol))
$(E)\text{-}CH_3CHCHOH + OH \rightarrow (E)\text{-}CH_3HC{=}CHOH\cdots O{-}H$ reac. 15	R^{-4}	0.267879 (Å^4·(kJ/mol))
$(Z)\text{-}CH_3CHCHOH + OH \rightarrow (Z)\text{-}CH_3HC{=}CHOH\cdots O{-}H$ reac. 16	R^{-4}	0.330949 (Å^4·(kJ/mol))
$CH_3OHCCH_2 + OH \rightarrow CH_3OHC{=}CH_2\cdots O{-}H$ reac. 17	R^{-4}	0.387263 (Å^4·(kJ/mol))
$CH_3OHCCH_2 + OH \rightarrow CH_3OHC{=}CH_2\cdots O{-}H$ reac. 18	R^{-4}	0.378257 (Å^4·(kJ/mol))
$HOHCCH_2(syn) + CN \rightarrow HOHC{-}CH_2(syn)\cdots CN$ reac. 19	R^{-4}	0.415288 (Å^4·(kJ/mol))
$HOHCCH_2(anti) + CN \rightarrow HOHCCH_2(anti)\cdots CN$ reac. 20	R^{-4}	0.262156 (Å^4·(kJ/mol))

between Langevin and Gorin models can usually provide a remarkable description of barrier-less reaction steps in the ISM, whose very low temperatures imply a leading role of the "outer" TS. When this is not the case, the generalized equations reported in the section devoted to theoretical background can be profitably employed. Of course, reactions involving large fragments require further investigation, but the fitting of radial quantum chemical potentials by polynomials of the squared inverse distance should retain its effectiveness.

Based on these premises, we will now try to develop a general and robust protocol for defining the most suitable interval of distances and placement of the sampling points in terms of the intrinsic characteristics of the reacting fragments. To this end, we report in Table 3 the covalent and van der Waals radii of all the atoms involved in the studied reactions.

Table 3. Covalent (from Ref 74) and van der Waals (from Ref 75) Radii (in Å) Employed in the Present Study

Atom	Covalent radius (Å)	van der Waals radius (Å)
H	0.31	1.10
C	0.73	1.70
N	0.71	1.55
O	0.66	1.52
S	1.05	1.80
Cl	0.99	1.75

Inspection of the radial potentials for all the studied reactions suggests that an interval ranging from 1.7 times the sum of covalent radii to twice the sum of van der Waals radii covers the sampled regions. The corresponding values of the distances between the closest atoms belonging to different fragments are collected in Table 4. Note that different choices of reference values for the covalent and van der Waals radii have a negligible effect on the final results.

A system-independent protocol can be obtained by introducing a variable X, which maps the original $[R_{min}, R_{max}]$ interval into its $[0, 1]$ counterpart

$$X = \frac{R - R_{min}}{R_{max} - R_{min}} \tag{29}$$

Then, the minimum number of points needed for an accurate fitting can be derived taking into account that the R^{-4} contribution always provides a fair description of the radial potential. Therefore, each computed electronic energy is assigned a weight Y proportional to the absolute value of the energy gradient at that point and normalized by the sum of the gradients. In this way, points with larger gradients will receive greater weight, with each point of this new array representing the portion of the total gradient change accounted for up to the corresponding normalized distance.

The points selected in this way for the whole set of 20 prototypical elementary reaction steps are shown in Section S4 (Samplings) of the Supporting Information, whereas a scatter plot of the normalized weights as a function of the normalized distances is shown in Figure 3.

As expected, a strong clustering of the data points is observed in the region $0.15 \leq X \leq 0.5$, indicating that this area requires more dense sampling since the largest variations of the intermolecular potentials occur within this intermediate range of normalized distances. The sparse distribution of points near the boundaries of the normalized distances ($X < 0.15$ and $X > 0.5$) suggests that the points at 0.0 and 1.0 relative normalized distances are sufficient for describing the potential behavior in these regions, while enforcing correct boundary conditions. While a general nonlinear spacing could offer some advantage, several additional tests showed that 5 electronic energy evaluations at normalized distances of 0.0, 0.2, 0.4, 0.6, and 1.0 are sufficient to define an accurate radial potential. Therefore, this general recipe can be confidently employed to characterize new unknown reactions with substantial

https://doi.org/10.1021/acs.jctc.4c01076
J. Chem. Theory Comput. XXXX, XXX, XXX−XXX

Table 4. Closest Atoms Belonging to Different Fragments, R_{min}, and R_{max} (in Å) for All the Studied Reactions

reaction label	closest atoms	R_{min} (Å)	R_{max} (Å)
$CH_3COOH + [NH_2]^+ \rightarrow [CH_3COHO\cdots NH_2]^+$ reac. 1	O−N	2.329	6.14
$[NH_2OH_2]^+ + HCONH_2 \rightarrow [NH_2OH{-}H\cdots OCHNH_2]^+$ reac. 2	O−H	1.649	5.34
$C_2H_4 \rightarrow C_2H_3 + H$ reac. 3	C−H	1.768	5.60
$CH_4 \rightarrow CH_3 + H$ reac. 4	C−H	1.768	5.60
$H_2S + Cl \rightarrow HSH\cdots Cl$ reac. 5	S−Cl	3.570	7.10
$H_2S + OH \rightarrow HSH\cdots OH$ reac. 6	S−O	2.907	6.64
$CH_2CHOH(anti) + OH \rightarrow CH_2CHO{-}H(anti)\cdots O{-}H$ reac. 7	O−H	1.649	5.34
$CH_2CHOH(anti) + OH \rightarrow H_2C{=}CHOH(anti)\cdots O{-}H$ reac. 8	C−O	2.363	6.44
$CH_2CHOH(anti) + OH \rightarrow CH_2CHH{-}O(anti)\cdots H{-}O$ reac. 9	O−H	1.649	5.34
$CH_2CHOH(syn) + OH \rightarrow H_2C{=}CHOH\cdots H{-}O$ reac. 10	C−O	2.363	6.44
$CH_2CHOH(syn) + OH \rightarrow H_2C{=}CHOH(syn)\cdots O{-}H$ reac. 11	C−O	2.363	6.44
$CH_2CHOH(syn) + OH \rightarrow H_2C{=}CHOH(syn)\cdots H{-}O$ reac. 12	C−O	2.363	6.44
$(E\text{-})CH_3CHCHOH + OH \rightarrow (E\text{-})CH_3CHCHO{-}H\cdots O{-}H$ reac. 13	C−O	2.363	6.44
$(Z\text{-})CH_3CHCHOH + OH \rightarrow (Z\text{-})CH_3CHCHO{-}H\cdots O{-}H$ reac. 14	C−O	2.363	6.44
$(E)\text{-}CH_3CHCHOH + OH \rightarrow (E)\text{-}CH_3HC{=}CHOH\cdots O{-}H$ reac. 15	C−O	2.363	6.44
$(Z)\text{-}CH_3CHCHOH + OH \rightarrow (Z)\text{-}CH_3HC{=}CHOH\cdots O{-}H$ reac. 16	C−O	2.363	6.44
$CH_3OHCCH_2 + OH \rightarrow CH_3OHC{=}CH_2\cdots O{-}H$ reac. 17	C−O	2.363	6.44
$CH_3OHCCH_2 + OH \rightarrow CH_3OHC{=}CH_2\cdots O{-}H$ reac. 18	C−O	2.363	6.44
$HOHCCH_2(syn) + CN \rightarrow HOHC{-}CH_2(syn)\cdots CN$ reac. 19	C−C	2.584	6.80
$HOHCCH_2(anti) + CN \rightarrow HOHCCH_2(anti)\cdots CN$ reac. 20	C−C	2.584	6.80

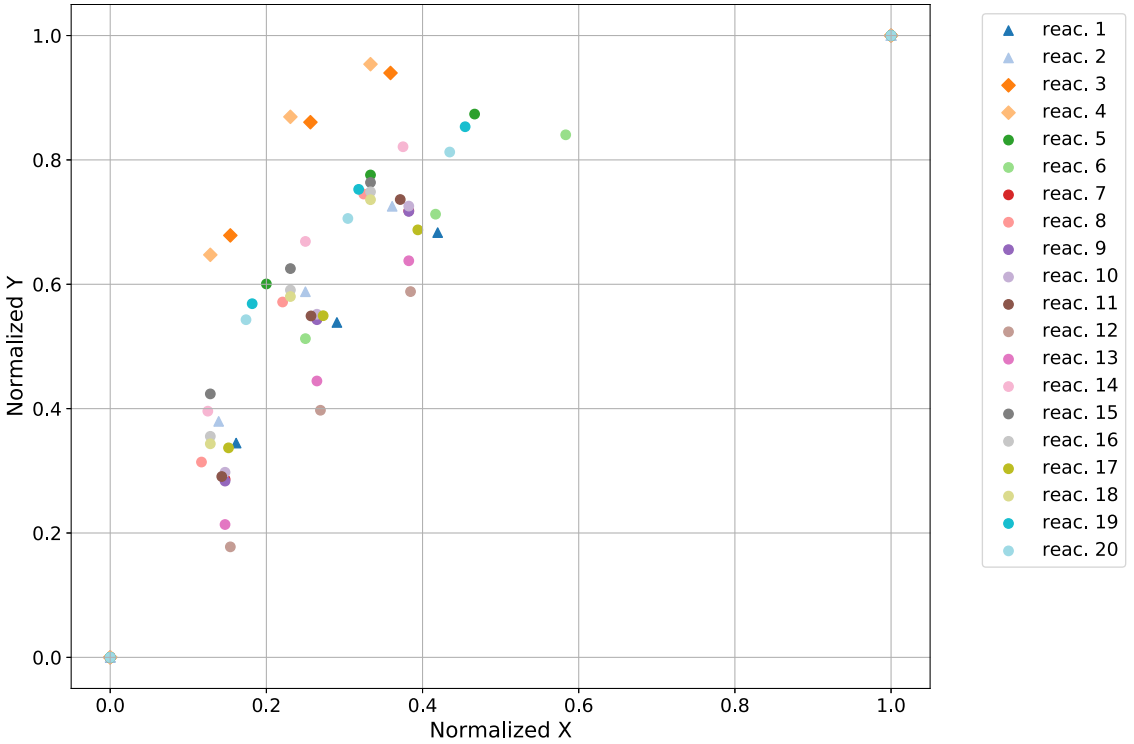

Figure 3. Optimal sampling points for fitting radial quantum chemical potentials. Each reaction is represented by a distinct color-coded marker. The horizontal and vertical axes refer to the relative normalized distances and energies (X and Y, respectively), both mapped in the [0, 1] interval.

reduction of computational cost and negligible accuracy decrease.

4. CONCLUSIONS

The present study introduces a novel computational protocol for the evaluation and fitting of reference radial potentials with special reference to barrier-less reaction steps in the gas-phase. The computed potentials can be employed either for obtaining reaction rates (by means of a generalized capture theory for processes ruled by outer transition states) or for improving LL results to be employed in the VRC-TST approach (for processes ruled by "inner" transition states or whenever both "outer" and "inner" transition states play a role).

A panel of 20 elementary reaction steps, involving ion−molecule, radical−molecule, and radical−radical interactions, has been characterized by accurate reduced-cost single-reference composite schemes (jun-ChS-F12 or CPCS3) including, when needed, spin splitting contributions by DDCI computations. The electronic energies computed at about 40 equi-spaced points covering a large region of the

https://doi.org/10.1021/acs.jctc.4c01076
J. Chem. Theory Comput. XXXX, XXX, XXX−XXX

reactive PES have been fitted by different polynomial expansions in terms of the squared inverse distance between the reacting centers. In most cases the R^{-4} contribution is sufficient to obtain a very good fit, with just a few reactions requiring the R^{-6} term, either alone or in addition to the R^{-4} term. Note that, even in these cases, the R^{-4} approximation performs well. This finding (which applies to both single- and multireference cases) paves the way toward the definition of a general protocol aimed to define a priori the region to be sampled and the minimum number of required points. As a matter of fact, the interval ranging from 1.7 times the sum of the covalent radii to twice the sum of the van der Waals radii of the closest atoms belonging to different fragments is sufficient for all the studied situations. Then, 5 points displaced by amounts related to the gradient of the leading R^{-4} term are sufficient for a robust and accurate fit.

Therefore, the way seems paved for the definition of an optimal black-box strategy for the study of barrier-less reaction steps. While further tests are surely needed for larger fragments, the present version of the proposed computational strategy already improves significantly the effectiveness and robustness of current approaches to this kind of problem.

■ ASSOCIATED CONTENT

Supporting Information

The Supporting Information is available free of charge at https://pubs.acs.org/doi/10.1021/acs.jctc.4c01076.

Additional data for all the reactions, including quantum chemical energies and the corresponding values obtained by different fitting recipes (PDF)

■ AUTHOR INFORMATION

Corresponding Author

Vincenzo Barone − *INSTM, Firenze 50121, Italy;* orcid.org/0000-0001-6420-4107; Email: vincebarone52@gmail.com

Authors

Luigi Crisci − *Scuola Normale Superiore di Pisa, Pisa I-56126, Italy;* orcid.org/0000-0002-8140-5397

Bernardo Ballotta − *School of Physics, Trinity College Dublin, Dublin 2, Ireland;* orcid.org/0000-0002-1591-9189

Marco Mendolicchio − *Scuola Normale Superiore di Pisa, Pisa I-56126, Italy;* orcid.org/0000-0002-4504-853X

Complete contact information is available at: https://pubs.acs.org/10.1021/acs.jctc.4c01076

Notes

The authors declare no competing financial interest.

■ ACKNOWLEDGMENTS

Funding from Gaussian Inc. is gratefully acknowledged.

■ REFERENCES

(1) Song, H.; Guo, H. Theoretical Insights into the Dynamics of Gas-Phase Bimolecular Reactions with Submerged Barriers. *ACS Phys. Chem. Au* **2023**, *3*, 406−418.

(2) Nuñez-Reyes, D.; Hickson, K. M. A Low Temperature Investigation of the Gas-Phase $N(^2D)$ + NO Reaction. Towards a Viable Source of $N(^2D)$ Atoms for Kinetic Studies in Astrochemistry. *Phys. Chem. Chem. Phys.* **2018**, *20*, 17442−17447.

(3) Ballotta, B.; Nandi, S.; Barone, V.; Rampino, S. Gas-Phase Formation and Isomerization Reactions of Cyanoacetaldehyde, a Prebiotic Molecule of Astrochemical Interest. *ACS Earth Space Chem.* **2021**, *5*, 1071−1082.

(4) Ballotta, B.; Marforio, T. D.; Rampino, S.; Martínez-Núñez, E.; Barone, V.; Melosso, M.; Bottoni, A.; Dore, L. Toward the Detection of Cyanoketene in the Interstellar Medium: New Hints from Quantum Chemistry and Rotational Spectroscopy. *ACS Earth Space Chem.* **2023**, *7*, 1172−1180.

(5) Sun, J.; Chu, H.; Wu, W.; Chen, F.; Sun, Y.; Liu, J.; Shao, Y.; Tang, Y. A Theoretical Study on Gas-Phase Reactions of Acrylic Acid with Chlorine Atoms: Mechanism, Kinetics, and Insights. *Environ. Sci. Pollut. Res.* **2020**, *27*, 15772−15784.

(6) Wang, H.; Zhao, M.; Zuo, Q.; Liu, M.; He, X.; Wang, Z.; Sun, Y.; Song, R.; Zhang, Y. A Theoretical Study of the Gas-Phase Reactions of Propadiene with NO_3: Mechanism, Kinetics and Insights. *RSC Adv.* **2023**, *13*, 21383−21392.

(7) Mondal, K.; Rajakumar, B. Experimental and Theoretical Investigation of Reactions of Formyl (HCO) Radicals in the Gas Phase: (I) Kinetics of HCO Radicals with Ethyl Formate and Ethyl Acetate in Tropospherically Relevant Conditions. *J. Phys. Chem. A* **2022**, *126*, 6135−6147.

(8) Zhang, P.; Ma, L.; Wang, H.; Li, H.; Song, R.; Wang, Z.; Sun, Y.; Zhang, Y. A Theoretical Study on Gas-Phase Reactions of CF_3CH = CF_2 with OH: Mechanism, Kinetics and Insights. *J. Fluorine Chem.* **2023**, *270*, 110168.

(9) Ern, A.; Giovangigli, V. Kinetic Theory of Reactive Gas Mixtures with Application to Combustion. *Transp. Theory Stat. Phys.* **2003**, *32*, 657−677.

(10) Wu, J.; Bruce, F. N. O.; Bai, X.; Ren, X.; Li, Y. Insights into the Reaction Kinetics of Hydrazine-Based Fuels: A Comprehensive Review of Theoretical and Experimental Methods. *Energies* **2023**, *16*, 6006.

(11) Konnov, A. A. Yet Another Kinetic Mechanism for Hydrogen Combustion. *Combust. Flame* **2019**, *203*, 14−22.

(12) Fernández-Ramos, A.; Miller, J. A.; Klippenstein, S. J.; Truhlar, D. G. Modeling the Kinetics of Bimolecular Reactions. *Chem. Rev.* **2006**, *106*, 4518−4584.

(13) Klippenstein, S. J.; Pande, V. S.; Truhlar, D. G. Chemical Kinetics and Mechanisms of Complex Systems: A Perspective on Recent Theoretical Advances. *J. Am. Chem. Soc.* **2014**, *136*, 528−546.

(14) Polino, D.; Klippenstein, S. J.; Harding, L. B.; Georgievskii, Y. Predictive Theory for the Addition and Insertion Kinetics of $^1CH_2$ Reacting with Unsaturated Hydrocarbons. *J. Phys. Chem. A* **2013**, *117*, 12677−12692.

(15) Zádor, J.; Taatjes, C. A.; Fernandes, R. X. Kinetics of Elementary Reactions in Low-Temperature Autoignition Chemistry. *Prog. Energy Combust. Sci.* **2011**, *37*, 371−421.

(16) Chesnavich, W. J.; Bass, L.; Su, T.; Bowers, M. T. Multiple Transition States in Unimolecular Reactions: A Transition State Switching Model. Application to the $C_4H_8^+$ System. *J. Chem. Phys.* **1981**, *74*, 2228−2246.

(17) Klippenstein, S. J.; Georgievskii, Y.; Harding, L. B. Statistical Theory for the Kinetics and Dynamics of Roaming Reactions. *J. Phys. Chem. A* **2011**, *115*, 14370−14381.

(18) Rai, S. N.; Truhlar, D. G. Variational Transition State Theory Calculations for an Atom−Radical Reaction With No Saddle Point: O +OH. *J. Chem. Phys.* **1983**, *79*, 6046−6059.

(19) Pechukas, P.; Light, J. C. On Detailed Balancing and Statistical Theories of Chemical Kinetics. *J. Chem. Phys.* **1965**, *42*, 3281−3291.

(20) Chesnavich, W. J. Multiple Transition States in Unimolecular Reactions. *J. Chem. Phys.* **1986**, *84*, 2615−2619.

(21) Georgievskii, Y.; Klippenstein, S. J. Long-range Transition State Theory. *J. Chem. Phys.* **2005**, *122*, 194103.

(22) Georgievskii, Y.; Klippenstein, S. J. Variable Reaction Coordinate Transition State Theory: Analytic Results and Application to the C_2H_3 + H → C_2H_4 Reaction. *J. Chem. Phys.* **2003**, *118*, 5442−5455.

(23) Klippenstein, S. J. A Bond Length Reaction Coordinate for Unimolecular Reactions. II. Microcanonical and Canonical Imple-

mentations with Application to the Dissociation of NCNO. *J. Chem. Phys.* **1991**, *94*, 6469−6482.
(24) Georgievskii, Y.; Klippenstein, S. J. Transition State Theory for Multichannel Addition Reactions: Multifaceted Dividing Surfaces. *J. Phys. Chem. A* **2003**, *107*, 9776−9781.
(25) Truhlar, D. G.; Garrett, B. C.; Klippenstein, S. J. Current Status of Transition-State Theory. *J. Phys. Chem.* **1996**, *100*, 12771−12800.
(26) Klippenstein, S. J. Implementation of RRKM Theory for Highly Flexible Transition States with a Bond Length as the Reaction Coordinate. *Chem. Phys. Lett.* **1990**, *170*, 71−77.
(27) Marcus, R. A. Generalization of the Activated Complex Theory of Reaction Rates. II. Classical Mechanical Treatment. *J. Chem. Phys.* **1964**, *41*, 2624−2633.
(28) Wardlaw, D. M.; Marcus, R. A. Unimolecular Reaction Rate Theory for Transition States of Partial Looseness. II. Implementation and Analysis with Applications to NO_2 and C_2H_6 Dissociations. *J. Chem. Phys.* **1985**, *83*, 3462−3480.
(29) Wardlaw, D. M.; Marcus, R. A. Unimolecular Reaction Rate Theory for Transition States of Any Looseness. 3. Application to Methyl Radical Recombination. *J. Phys. Chem.* **1986**, *90*, 5383−5393.
(30) Crisci, L.; Di Grande, S.; Cavallotti, C.; Barone, V. Toward an Accurate Black-Box Tool for the Kinetics of Gas-Phase Reactions Involving Barrier-less Elementary Steps. *J. Chem. Theory Comput.* **2023**, *19*, 7626−7639.
(31) Zhou, C.-W.; Simmie, J. M.; Curran, H. J. Rate Constants for Hydrogen-Abstraction by ȮH from *n*-Butanol. *Combust. Flame* **2011**, *158*, 726−731.
(32) Nurkowski, D.; Klippenstein, S. J.; Georgievskii, Y.; Verdicchio, M.; Jasper, A. W.; Akroyd, J.; Mosbach, S.; Kraft, M. Ab Initio Variational Transition State Theory and Master Equation Study of the Reaction $(OH)_3$ $SiOCH_2$ + CH_3⇌$(OH)_3$ $SiOC_2H_5$. *Z. Phys. Chem.* **2015**, *229*, 691−708.
(33) Crisci, L.; Barone, V. Reconciling Accuracy and Feasibility for Barrierless Reaction Steps by the PCS/DDCI/MC-PDFT Protocol: Methane and Ethylene Dissociations as Case Studies. *J. Chem. Theory Comput.* **2024**, *20*, 8539−8548.
(34) Zhang, Z. P.; Wang, S. H.; Shang, Y. L.; Liu, J. H.; Luo, S. N. Theoretical Study on Ethylamine Dissociation Reactions Using VRC-VTST and SS-QRRK Methods. *J. Phys. Chem. A* **2024**, *128*, 2191−2199.
(35) Barone, V.; Lupi, J.; Salta, Z.; Tasinato, N. Reliable Gas Phase Reaction Rates at Affordable Cost by Means of the Parameter-Free JunChS-F12 Model Chemistry. *J. Chem. Theory Comput.* **2023**, *19*, 3526−3537.
(36) Barone, V.; Crisci, L.; Di Grande, S. Accurate Thermochemical and Kinetic Parameters at Affordable Cost by Means of the Pisa Composite Scheme (PCS). *J. Chem. Theory Comput.* **2023**, *19*, 7273−7286.
(37) García, V. M.; Castell, O.; Caballol, R.; Malrieu, J. An Iterative Difference-Dedicated Configuration Interaction. Proposal and Test Studies. *Chem. Phys. Lett.* **1995**, *238*, 222−229.
(38) Cabrero, J.; de Graaf, C.; Bordas, E.; Caballol, R.; Malrieu, J.-P. Role of the Coordination of the Azido Bridge in the Magnetic Coupling of Copper(II) Binuclear Complexes. *Chem.—Eur. J.* **2003**, *9*, 2307−2315.
(39) Miralles, J.; Castell, O.; Caballol, R.; Malrieu, J.-P. Specific CI Calculation of Energy Differences: Transition Energies and Bond Energies. *Chem. Phys.* **1993**, *172*, 33−43.
(40) Calzado, C. J.; Cabrero, J.; Malrieu, J. P.; Caballol, R. Analysis of the Magnetic Coupling in Binuclear Complexes. I. Physics of the Coupling. *J. Chem. Phys.* **2002**, *116*, 2728−2747.
(41) Calzado, C. J.; Angeli, C.; Caballol, R.; Malrieu, J.-P. Extending the Active Space in Multireference Configuration Interaction Calculations of Magnetic Coupling Constants. *Theor. Chem. Acc.* **2010**, *126*, 185−196.
(42) Kaplan, I. G. *Intermolecular Interactions*; John Wiley & Sons, Ltd., 2006; Chapter 2, pp 25−79.
(43) Bernstein, R. B. In *Atom−Molecule Collision Theory: A Guide for the Experimentalist*; Bernstein, R. B., Ed.; Springer US: Boston, MA, 1979; pp 1−43.
(44) Langevin, P. M. Une Formule Fondamentale de Théorie Cinétique. *Ann. Chim. Phys.* **1905**, *5*, 245.
(45) Gorin, E. Photolysis of Aldehydes and Ketones in the Presence of Iodine Vapor. *J. Chem. Phys.* **1939**, *7*, 256−264.
(46) Szabó, Z. G. *Fortschritte in der Kinetik der Homogenen Gasreaktionen*; Steinkopff: Heidelberg, 1961; pp 39−71.
(47) Garrett, B. C.; Truhlar, D. G. Criterion of Minimum State Density in the Transition State Theory of Bimolecular Reactions. *J. Chem. Phys.* **1979**, *70*, 1593−1598.
(48) Tsikritea, A.; Diprose, J. A.; Softley, T. P.; Heazlewood, B. R. Capture Theory Models: An Overview of Their Development, Experimental Verification, and Applications to Ion−Molecule Reactions. *J. Chem. Phys.* **2022**, *157*, 060901.
(49) Eliason, M. A.; Hirschfelder, J. O. General Collision Theory Treatment for the Rate of Bimolecular, Gas Phase Reactions. *J. Chem. Phys.* **1959**, *30*, 1426−1436.
(50) Di Grande, S.; Barone, V. Toward Accurate Quantum Chemical Methods for Molecules of Increasing Dimension: the New Family of Pisa Composite Schemes. *J. Phys. Chem. A* **2024**, *128*, 4886−4900.
(51) Peterson, K. A.; Dunning, T. H., Jr. Accurate Correlation Consistent Basis Sets for Molecular Core−Valence Correlation Effects: The Second Row Atoms Al−Ar, and the First Row Atoms B−Ne Revisited. *J. Chem. Phys.* **2002**, *117*, 10548−10560.
(52) Papajak, E.; Zheng, J.; Xu, X.; Leverentz, H. R.; Truhlar, D. G. Perspectives on Basis Sets Beautiful: Seasonal Plantings of Diffuse Basis Functions. *J. Chem. Theory Comput.* **2011**, *7*, 3027−3034.
(53) Peterson, K. A.; Adler, T. B.; Werner, H.-J. Systematically Convergent Basis Sets for Explicitly Correlated Wavefunctions: the Atoms H, He, B−Ne, and Al−Ar. *J. Chem. Phys.* **2008**, *128*, 084102.
(54) Barone, V.; Di Grande, S.; Lazzari, F.; Mendolicchio, M. Accurate Structures and Spectroscopic Parameters of Guanine Tautomers in the Gas Phase by the Pisa Conventional and Explicitly Correlated Composite Schemes (PCS and PCS-F12). *J. Phys. Chem. A* **2023**, *127*, 6771−6778.
(55) Cacelli, I.; Ferretti, A.; Prampolini, G.; Barone, V. BALOO: a Fast and Versatile Code for Accurate Multi-Reference Variational/Perturbative Calculations. *J. Chem. Theory Comput.* **2015**, *11*, 2024−2035.
(56) Miralles, J.; Daudey, J.-P.; Caballol, R. Variational Calculation of Small Energy Differences. The Singlet-Triplet Gap in $[Cu_2Cl_6]^{2-}$. *Chem. Phys. Lett.* **1992**, *198*, 555−562.
(57) Barone, V.; Cacelli, I.; Ferretti, A.; Monti, S.; Prampolini, G. An Integrated Protocol for the Accurate Calculation of Magnetic Interactions in Organic Magnets. *J. Chem. Theory Comput.* **2011**, *7*, 699−706.
(58) Werner, H.-J.; Knowles, P. J.; Manby, F. R.; Black, J. A.; Doll, K.; Heßelmann, A.; Kats, D.; Köhn, A.; Korona, T.; Kreplin, D. A.; Ma, Q.; Miller, T. F., III; Mitrushchenkov, A.; Peterson, K. A.; Polyak, I.; Rauhut, G.; Sibaev, M.; Sibaev, M. The Molpro Quantum Chemistry Package. *J. Chem. Phys.* **2020**, *152*, 144107.
(59) Puzzarini, C.; Bloino, J.; Tasinato, N.; Barone, V. Accuracy and Interpretability: The Devil and the Holy Grail. New Routes across Old Boundaries in Computational Spectroscopy. *Chem. Rev.* **2019**, *119*, 8131−8191.
(60) Barone, V.; Puzzarini, C.; Mancini, G. Integration of theory, simulation, artificial intelligence and virtual reality: a four-pillar approach for reconciling accuracy and interpretability in computational spectroscopy. *Phys. Chem. Chem. Phys.* **2021**, *23*, 17079−17096.
(61) Uribe, L.; Di Grande, S.; Crisci, L.; Lazzari, F.; Mendolicchio, M.; Barone, V. Accurate Structures and Rotational Constants of Steroid Hormones at DFT Cost: Androsterone, Testosterone, Estrone, β-Estradiol, and Estriol. *J. Phys. Chem. A* **2024**, *128*, 2629−2642.
(62) Uribe, L.; Lazzari, F.; Di Grande, S.; Crisci, L.; Mendolicchio, M.; Barone, V. Accurate structures and rotational constants of bicyclic

https://doi.org/10.1021/acs.jctc.4c01076
J. Chem. Theory Comput. XXXX, XXX, XXX−XXX

monoterpenes at DFT cost by means of the bond-corrected Pisa composite scheme (BPCS). *J. Chem. Phys.* **2024**, *161*, 014307.
(63) Santra, G.; Sylvetsky, N.; Martin, J. M. L. Minimally Empirical Double-Hybrid Functionals Trained against the GMTKN55 Database: revDSD-PBEP86-D4, revDOD-PBE-D4, and DOD-SCAN-D4. *J. Phys. Chem. A* **2019**, *123*, 5129−5143.
(64) Frisch, M. J.; Trucks, G. W.; Schlegel, H. B.; Scuseria, G. E.; Robb, M. A.; Cheeseman, J. R.; Scalmani, G.; Barone, V.; Petersson, G. A.; Nakatsuji, H.; Li, X.; Caricato, M.; Marenich, A. V.; Bloino, J.; Janesko, B. G.; Gomperts, R.; Mennucci, B.; Hratchian, H. P.; Ortiz, J. V.; Izmaylov, A. F.; Sonnenberg, J. L.; Williams-Young, D.; Ding, F.; Lipparini, F.; Egidi, F.; Goings, J.; Peng, B.; Petrone, A.; Henderson, T.; Ranasinghe, D.; Zakrzewski, V. G.; Gao, J.; Rega, N.; Zheng, G.; Liang, W.; Hada, M.; Ehara, M.; Toyota, K.; Fukuda, R.; Hasegawa, J.; Ishida, M.; Nakajima, T.; Honda, Y.; Kitao, O.; Nakai, H.; Vreven, T.; Throssell, K.; Montgomery, J. A.; Peralta, J. E.; Ogliaro, F.; Bearpark, M. J.; Heyd, J. J.; Brothers, E. N.; Kudin, K. N.; Staroverov, V. N.; Keith, T. A.; Kobayashi, R.; Normand, J.; Raghavachari, K.; Rendell, A. P.; Burant, J. C.; Iyengar, S. S.; Tomasi, J.; Cossi, M.; Millam, J. M.; Klene, M.; Adamo, C.; Cammi, R.; Ochterski, J. W.; Martin, R. L.; Morokuma, K.; Farkas, O.; Foresman, J. B.; Fox, D. J. *Gaussian 16, Revision C.01*; Gaussian, Inc.: Wallingford CT, 2016.
(65) Largo, L.; Rayón, V. M.; Barrientos, C.; Largo, A.; Redondo, P. Gas-Phase Reaction of NH2(+) with Acetic Acid: Implications in Astrochemistry. *J. Chem. Theory Comput.* **2008**, *4*, 2085−2093.
(66) Brigiano, F. S.; Jeanvoine, Y.; Largo, A.; Spezia, R. The Formation of Urea in Space-I. Ion−Molecule, Neutral-Neutral, and Radical Gas-Phase Reactions. *Astron. Astrophys.* **2018**, *610*, A26.
(67) Ballotta, B.; Martínez-Núñez, E.; Rampino, S.; Barone, V. Competition Between Abstraction and Addition Channels for the Reaction Between the OH Radical and Vinyl Alcohol in the Interstellar Medium. *ACS Earth Space Chem.* **2023**, *7*, 1467−1477.
(68) Tishchenko, O.; Ilieva, S.; Truhlar, D. G. Communication: Energetics of Reaction Pathways for Reactions of Ethenol with the Hydroxyl Radical: The Importance of Internal Hydrogen Bonding at the Transition State. *J. Chem. Phys.* **2010**, *133*, 021102.
(69) Rösch, D.; Jones, G. H.; Almeida, R.; Caravan, R. L.; Hui, A.; Ray, A. W.; Percival, C. J.; Sander, S. P.; Smarte, M. D.; Winiberg, F. A. F.; Okumura, M.; Osborn, D. L. Conformer-Dependent Chemistry: Experimental Product Branching of the Vinyl Alcohol + OH + O_2 Reaction. *J. Phys. Chem. A* **2023**, *127*, 3221−3230.
(70) Lei, X.; Wang, W.; Cai, J.; Wang, C.; Liu, F.; Wang, W. Atmospheric Chemistry of Enols: Vinyl Alcohol + OH + O_2 Reaction Revisited. *J. Phys. Chem. A* **2019**, *123*, 3205−3213.
(71) Zhou, C.-W.; Mebel, A. M.; Li, X.-Y. An ab Initio/Rice-Ramsperger-Kassel-Marcus Study of the Reactions of Propenols with OH. Mechanism and Kinetics of H Abstraction Channels. *J. Phys. Chem. A* **2009**, *113*, 10667−10677.
(72) Lei, X.; Chen, D.; Wang, W.; Liu, F.; Wang, W. Quantum Chemical Studies of the OH-Initiated Oxidation Reactions of Propenols in the Presence of O_2. *Mol. Phys.* **2019**, *117*, 682−692.
(73) Ballotta, B.; Martínez-Núñez, E.; Rampino, S.; Barone, V. New Prebiotic Molecules in the Interstellar Medium from the Reaction Between Vinyl Alcohol and CN Radicals: Unsupervised Reaction Mechanism Discovery, Accurate Electronic Structure Calculations and Kinetic Simulations. *Phys. Chem. Chem. Phys.* **2023**, *25*, 22840−22850.
(74) Pauling, L. The Nature of the Chemical Bond. II. The One-Electron Bond and the Three-Electron Bond. *J. Am. Chem. Soc.* **1931**, *53*, 3225−3237.
(75) Mantina, M.; Chamberlin, A. C.; Valero, R.; Cramer, C. J.; Truhlar, D. G. Consistent van der Waals Radii for the Whole Main Group. *J. Phys. Chem. A* **2009**, *113*, 5806−5812.

https://doi.org/10.1021/acs.jctc.4c01076
J. Chem. Theory Comput. XXXX, XXX, XXX−XXX